

# SCIENTIFIC REPORTS



OPEN

## Suppressing epileptic activity in a neural mass model using a closed-loop proportional-integral controller

Received: 15 October 2015

Accepted: 18 May 2016

Published: 07 June 2016

Junsong Wang<sup>1</sup>, Ernst Niebur<sup>2</sup>, Jinyu Hu<sup>3</sup> & Xiaoli Li<sup>4</sup>

Closed-loop control is a promising deep brain stimulation (DBS) strategy that could be used to suppress high-amplitude epileptic activity. However, there are currently no analytical approaches to determine the stimulation parameters for effective and safe treatment protocols. Proportional-integral (PI) control is the most extensively used closed-loop control scheme in the field of control engineering because of its simple implementation and perfect performance. In this study, we took Jansen's neural mass model (NMM) as a test bed to develop a PI-type closed-loop controller for suppressing epileptic activity. A graphical stability analysis method was employed to determine the stabilizing region of the PI controller in the control parameter space, which provided a theoretical guideline for the choice of the PI control parameters. Furthermore, we established the relationship between the parameters of the PI controller and the parameters of the NMM in the form of a stabilizing region, which provided insights into the mechanisms that may suppress epileptic activity in the NMM. The simulation results demonstrated the validity and effectiveness of the proposed closed-loop PI control scheme.

Epilepsy is thought to be a dynamical disorder of the brain at the systems level<sup>1–3</sup>, which makes it particularly suitable to be studied from the perspectives of computational modelling and system theory<sup>1,4,5</sup>. Closed-loop control is a promising deep brain stimulation (DBS) strategy for suppressing abnormal neural activities, such as epilepsy and Parkinson's disease, and it has thus become the focus of current experimental and theoretical studies<sup>6–18</sup>.

Control theory is an emerging method that is used to develop closed-loop controllers for suppressing epileptic seizures<sup>11</sup>, and some advanced control strategies are involved in the design of closed-loop DBS control<sup>10,13,14</sup>. A closed-loop controller was developed based on a recursively identified autoregressive model that described the relationship between stimulation input and local field potential output<sup>10</sup>. A responsive neuron modulator, based on a radial basis function neural network, was employed to control seizure-like events in a computational model of epilepsy<sup>13</sup>. In addition, optimal control theory was used to design a desynchronizing control stimulus for a network of pathologically synchronized neurons<sup>14</sup>. Although these control schemes performed excellently, the control algorithms were somewhat complex. These results suggest that a simple control algorithm may be preferred in closed-loop control of epileptic activity.

A proportional-integral-derivative (PID) controller is the most extensively used closed-loop controller in the field of control engineering because of its simple implementation and robust performance<sup>19</sup>. In this context, the PID-type controller was introduced to control various pathological neural activities<sup>12,20–23</sup>. Proportional and proportional-derivative amplitude control were proposed for the closed-loop DBS of patients with Parkinson's disease<sup>24</sup>. Proportional feedback stimulation was employed to control seizures in rats<sup>25</sup>. Integral feedback control was developed for the charge-balanced suppression of epileptic seizures<sup>26</sup> and the modulation of brain rhythms in Parkinson's disease<sup>27</sup>. Proportional controllers, differential controllers and filter controllers were used to eliminate seizing activity in a mathematical model of human cortical, electrical activity<sup>28</sup>. A reactive and adaptive control

<sup>1</sup>School of Biomedical Engineering, Tianjin Medical University, Tianjin 300070, China. <sup>2</sup>Zanvyl Krieger Mind/Brain Institute and Solomon Snyder Department of Neuroscience, Johns Hopkins University, Baltimore, MD 21218, USA.

<sup>3</sup>Division of Immunology and Rheumatology, Department of Medicine, Stanford University, Stanford, CA 94305, USA. <sup>4</sup>National Key Laboratory of Cognitive Neuroscience and Learning, Beijing Normal University, Beijing 100875, China. Correspondence and requests for materials should be addressed to J.W. (email: wjsong2004@126.com) or X.L. (email: xiaoli@bnu.edu.cn)

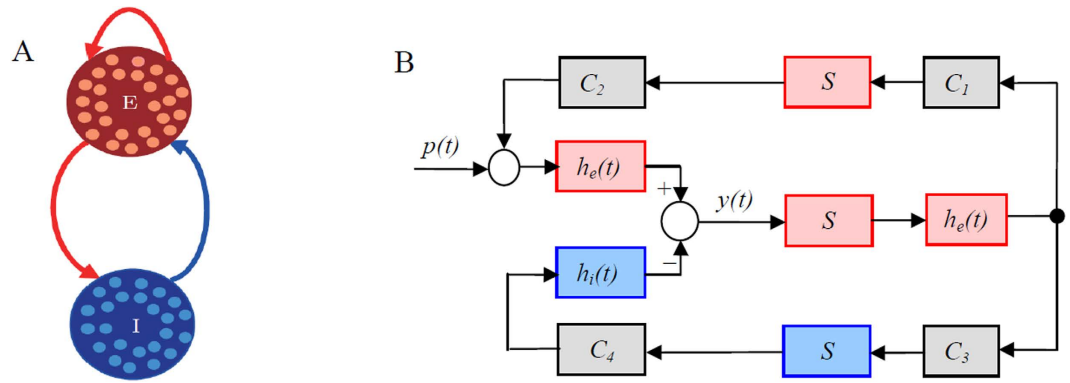


**Figure 1. Structure of the neural mass model.** (A) The schematic diagram of the NMM. “E” and “I” represent excitatory and inhibitory subpopulations, respectively, that are defined as groups of statistically similar excitatory or inhibitory neurons that share the same inputs and connectivity. (B) Block diagram of the NMM. The red and blue blocks correspond to excitatory and inhibitory subpopulations, respectively.

scheme was proposed to suppress epileptiform discharges in realistic, computational, neuronal models with bistability<sup>29</sup>. In this model, the cumulative sum of the difference between the measured ictality and the pre-defined acceptable limit over all previous epochs was used to determine the modulating factor for the instantaneous stimulation strength during the current epoch. Therefore, the control scheme was, in essence, integral feedback control in a discrete form. Furthermore, delayed feedback control is another representative control scheme that has been used to suppress pathological brain rhythms by desynchronizing the neural activities<sup>30,31</sup>.

PID-type controllers have achieved great success in controlling various pathological neural activities. However, the control parameters are currently chosen empirically by using a “trial and error” approach. This makes the outcome strongly dependent on the designer’s experience. Additionally, the work is time-consuming and its efficiency is not guaranteed, which makes the choice of control parameters quite challenging. Thus, an analytical design method of the PID-type controller is urgently needed. Furthermore, because epilepsy is caused by an unbalance between excitation and inhibition<sup>32</sup>, the control parameters should be related to the excitatory and inhibitory parameters. However, it still remains unclear how to build a quantitative relationship between the two sides.

Computational models have become attractive due to their ability to model complex neurological phenomena with relative ease<sup>1,33–35</sup>. A neural mass model is based on a biologically plausible parameterization of the layered neocortex dynamic behaviour. Neural mass model was initially proposed to study the origin of the alpha rhythm, and subsequently improved and extended to describe more general cortical, electrical activities<sup>34</sup>, such as electroencephalogram (EEG)<sup>36,37</sup>, functional magnetic resonance imaging (fMRI) signals<sup>38</sup> and event-related potentials<sup>39</sup>. Specifically, the NMM was successfully used to generate epileptic activity similar to that experimentally observed<sup>40–43</sup>. Jansen’s neural mass model (NMM) is characterized by the interaction of the interlinked excitatory and inhibitory feedback loops<sup>44</sup>. Previous studies have demonstrated that Jansen’s NMM can generate high-amplitude epileptic activity caused by the abnormal values of the external input<sup>43,45</sup> and the connection strength of the model<sup>41</sup>. Our recent bifurcation study found that the imbalance of the excitatory and inhibitory feedback loops in Jansen’s NMM resulted in the generation of high-amplitude epileptic activity<sup>42</sup>. Therefore, we used Jansen’s NMM as a test bed to develop the closed-loop PI controller for suppressing epileptic activity in the model (for simplicity, we use NMM to represent Jansen’s NMM in the remainder of this article).

Here, we used feedback control theory to develop a proportional-integral (PI) controller to suppress the high-amplitude epileptic activity in the NMM. A graphical stability analysis method was employed to determine the stabilizing region of the PI controller in the control parameter space. Our main goal was to develop an analytical design method for a PI controller that suppresses epileptic activity and to provide theoretical guidelines for choosing PI control parameters. If the PI controller stabilizing region was known for a given set of excitatory and inhibitory parameters of the NMM, then the time-consuming stability check for each set of control parameters could be avoided and the PI controller tuning time could be reduced. Furthermore, we determined the relationship between the parameters of the PI controller and the excitatory and inhibitory parameters of the NMM in the form of a stabilizing region, which was helpful for understanding the mechanism of suppressing epileptic activity.

## Methods

**Model.** The schematic and block diagram of the NMM is shown in Fig. 1A,B<sup>44</sup>, respectively. The NMM was composed of the following three interacting subpopulations: the main subpopulation (middle part), the excitatory (top part) and inhibitory (bottom part) feedback subpopulations.  $C_1$ ,  $C_2$ ,  $C_3$  and  $C_4$  are connectivity constants that represent interactions between the subpopulations and characterize the average numbers of synaptic contacts;  $p(t)$  is the input of the NMM and modelled by Gaussian noise; and  $y(t)$  is the output of the NMM, corresponding to the average synaptic activity of the pyramidal cells, that is interpreted as an EEG signal.

Each subpopulation of the NMM was composed of an excitatory,  $h_e(t)$ , or inhibitory synaptic dynamic function,  $h_i(t)$ , and a sigmoid static function,  $S(v)$ . The synaptic functions,  $h_e(t)$  and  $h_i(t)$ , transform the average pre-synaptic firing rates into average post-synaptic membrane potentials and are defined as  $h_e(t) = H_e e^{-|I\tau_e|/\tau_e}$

| Parameter     | Description   | Standard value   |
|---------------|---|--|
| $H_e$         | average excitatory synaptic gain                                    | 3.25 mV  |
| $H_i$         | average inhibitory synaptic gain                                    | 22 mV  |
| $\tau_e$      | average synaptic time constant for excitatory subpopulation         | 0.0108 s   |
| $\tau_i$      | average synaptic time constant for inhibitory subpopulation         | 0.02 s   |
| $C_1, C_2$    | average number of synaptic contacts in the excitatory feedback loop | $C_1 = 135; C_2 = 0.8 \times 135$  |
| $C_3, C_4$    | average number of synaptic contacts in the inhibitory feedback loop | $C_3 = 0.25 \times 135; C_4 = 0.25 \times 135$                           |
| $v_0, e_0, r$ | parameters of nonlinear S function                                  | $v_0 = 6 \text{ mV}; e_0 = 2.5 \text{ s}^{-1}; r = 0.56 \text{ mV}^{-1}$ |

**Table 1. Physiological interpretation and standard values of the parameters in the NMM.**

and  $h_i(t) = H_i t e^{-t/\tau_i} / \tau_i^{44}$ , where  $H_e$  and  $H_i$  represent the excitatory and inhibitory synaptic strengths and  $\tau_e$  and  $\tau_i$  are the membrane time constants. The sigmoid function,  $S(v)$ , transforms the average membrane potential into the average firing rate and is defined as  $S(v) = 2e_0 / [1 + e^{r(v_0 - v)}]^{46}$ , where  $2e_0$  is the maximum firing rate,  $v_0$  is the post-synaptic potential corresponding to a firing rate of  $e_0$ , and  $r$  describes the steepness of the sigmoid function. The parameter values of the NMM are listed in Table 1<sup>44</sup>.

**Graphical stability analysis method.** A graphical stability analysis method was employed to determine the stabilizing region of PI controller for suppressing epileptic activity in the NMM. The key point of designing the PI controller was to choose the control parameter values such that homeostasis of the NMM was maintained. To achieve this objective, we wanted to determine the stabilizing region of the PI controller.

If it is assumed that the characteristic polynomial of one control system is denoted as  $\Delta(s)$ , then all of the coefficients of  $\Delta(s)$  are real; therefore, the characteristic roots of  $\Delta(s)$  must be complex conjugates. According to linear stability theory<sup>47</sup>, the stability boundary of the control system is defined by  $\Delta(j\omega) = 0$ . Hence, it is sufficient to consider the following two cases:  $\omega = 0$  and  $\omega \in (0, \infty)$ . The stability boundary of the control system was defined as follows<sup>48</sup>:

$$H = H_1 U H_2, \quad (1)$$

where

$$\begin{aligned} H_1 &= \{(\Omega_1) | \Delta(j\omega; \Omega_1) = 0, \omega = 0\}, \\ H_2 &= \{(\Omega_2) | \Delta(j\omega; \Omega_2) = 0, \forall \omega \in (0, \infty)\}. \end{aligned}$$

where  $\Omega_1$  and  $\Omega_2$  represent the control parameter sets of the employed controller to be determined for the two cases  $\omega = 0$  and  $\omega \in (0, \infty)$ , respectively. In this study, Equation (1) was utilized to determine the stabilizing region of the PI controller in the control parameters space.

## Results and Discussion

**Control Scheme.** The control scheme was developed based on the fact that epileptic activity can be characterized as high-amplitude limit cycle oscillation born in Hopf bifurcation<sup>4,28,31,33,36,41,42,49–53</sup>, which indicates that the fixed point of the NMM lost its stability. Thus, we aimed to design a PI controller to stabilize the unstable, fixed point to prevent the generation of the Hopf bifurcation and to further suppress high-amplitude epileptic activity.

Epilepsy is thought to be caused by an imbalance between excitation and inhibition resulted from hyper-excitation or low inhibition<sup>32</sup>. Thus, the design objective was to determine the PI controller parameter values that stabilized the unstable NMM caused by abnormally large excitatory or small inhibitory parameter values<sup>32,42</sup> such that homeostasis of the NMM was maintained and the high-amplitude epileptic activity was suppressed. To do that, we employed a graphical stability analysis method that determined the stabilizing region of the PI controller in the parameter space.

The proposed PI control scheme for suppressing epileptic activity is shown in Fig. 2A, where  $u(t)$  is the output of PI controller, corresponding to the electrical stimulation signals, and  $y(t)$  represents the local field potential of a neural mass. The local electrical field in the neural mass was measured by the recording electrode and feeds back to the PI controller via the stimulating electrode. By using the NMM to model activity of the neural mass in Fig. 2A, we derived the block diagram of the proposed control scheme, shown in Fig. 2B, where  $y(t)$  is the output of the NMM and  $u(t)$  is the output of the PI controller.

To take advantage of the graphical stability analysis method used to design the PI controller, we replaced the nonlinear sigmoid function,  $S(v)$ , with its linear approximation around the equilibrium point,  $v = v_0$ , as follows:

$$K_s = S'(v) \Big|_{v=v_0} = \frac{2e_0 r e^{r(v_0 - v)}}{[1 + e^{r(v_0 - v)}]^2} \Big|_{v=v_0} = \frac{e_0 r}{2}, \text{ where } S'(v) \text{ represents the derivative of } S(v).$$

According to Fig. 2B, we derived the transfer function of the NMM as follows:

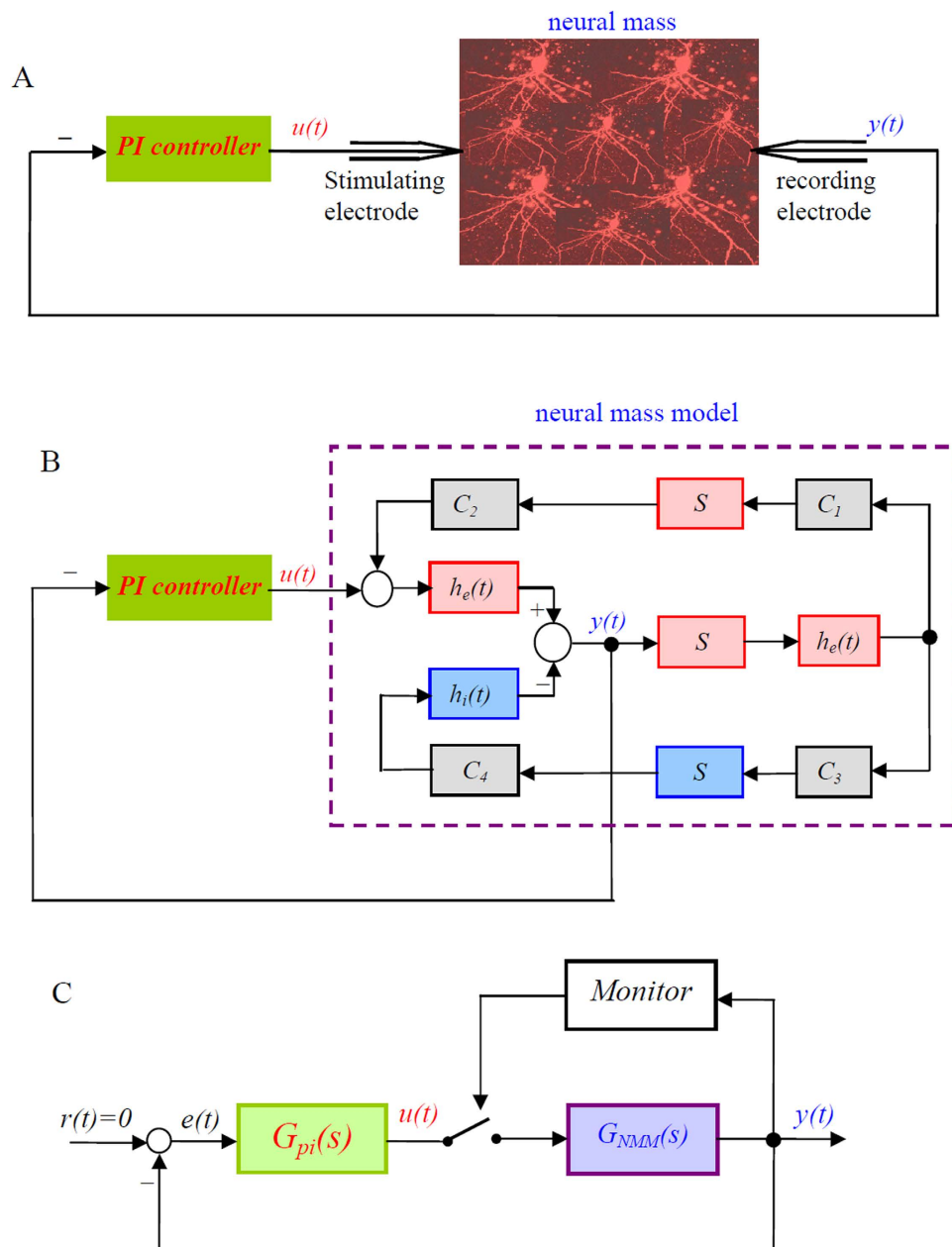


**Figure 2. The proposed PI control scheme for suppressing epileptic activity in the NMM.** (A) Schematic diagram of the PI-based control scheme. (B) Block diagram of the PI-based control scheme that modelled the activities of the neural mass using the NMM. The purple dashed block represents the NMM. (C) The simplified equivalent form of the proposed PI control scheme that replaced the purple dashed block in Fig. 2B with the transfer function  $G_{NMM}(s)$  of the NMM.

$$G_{NMM}(s) = \frac{Y(s)}{U(s)} = \frac{G_e(s)}{1 + K_s^2 G_e(s) [C_3 C_4 G_i(s) - C_1 C_2 G_e(s)]}, \quad (2)$$

where  $Y(s)$  and  $U(s)$  are the Laplace transform of  $y(t)$  and  $u(t)$ , respectively.  $G_e(s) = \frac{H_e \tau_e}{(\tau_e s + 1)^2}$  and  $G_i(s) = \frac{H_i \tau_i}{(\tau_i s + 1)^2}$  are the Laplace transform of  $h_e(t)$  and  $h_i(t)$  in the NMM, respectively.

Figure 2B can be simplified as a standard form of typical control systems, shown in Fig. 2C, where  $r(t)$  is the desired output of the NMM,  $e(t)$  is the error signal of the closed-loop control system and the system is defined as  $e(t) = r(t) - y(t)$ . For simplicity, in the remainder of the article, we will use PI-NMM to represent the closed-loop control system composed of the PI controller and the NMM.

In addition to epileptic activity, the NMM may feature multiple parallel states, such as low-amplitude oscillation and fluctuation output at a fixed point<sup>33,50,51,54,55</sup>. Thus, as shown in Fig. 2C, the feedback loop was closed

only when the amplitude of the output of the NMM exceeded a predetermined threshold. Correspondingly, the control signal  $u(t)$  is defined as

$$u(t) = \begin{cases} K_p e(t) + K_i \int e(t) dt, & \text{amplitude} > A_0 \\ 0, & \text{otherwise} \end{cases} \tag{3}$$

where  $K_p$  and  $K_i$  are the proportional and integral coefficients of the PI controller, respectively.  $A_0$  is the predetermined amplitude threshold beyond which stimulation is applied.

By conducting a Laplace transform of Equation (3), we can obtain the transfer function of the PI controller as follows:

$$G_{pi}(s) = \frac{U(s)}{E(s)} = K_p + \frac{K_i}{s}, \tag{4}$$

where  $E(s)$  is the Laplace transform of the error signal,  $e(t)$ .

According to feedback control principles<sup>47</sup>, the control objective of a feedback control system is to make the error signal  $e(t) \rightarrow 0$ . This indicates that the output of the PI-NMM control system will approach the desired output under the control of the PI controller, i.e.,  $y(t) \rightarrow r(t)$ . In this study, our goal in implementing the PI controller was to suppress the high-amplitude epileptic activity in the NMM; thus, the desired output of the PI-NMM control system was set to zero, i.e.,  $r(t) = 0$ .

**Theoretical results of the stability analysis.** To determine the stabilizing region of the PI controller in the  $(K_p, K_i)$  parameter space in which the PI-NMM control system was stable, we used the graphical stability analysis method to determine the stability boundary of the PI controller in the  $K_p, K_i$  plane.

According to Fig. 2C, we can derive the characteristic equation of the PI-NMM control system as

$$\Delta(s) = 1 + G_{pi}(s)G_{NMM}(s) = 0, \tag{5}$$

where  $\Delta(s)$  is the characteristic polynomial of the PI-NMM control system.

Defining  $s = j\omega$  and substituting it into Equation (5), one can obtain

$$\Delta(j\omega) = 1 + G_{pi}(j\omega)G_{NMM}(j\omega) = 0, \tag{6}$$

Equation (6) defines the stability boundary of the PI-NMM control system.

According to the graphical stability analysis method shown in Equation (1), we can discuss the two cases  $\omega = 0$  and  $\omega > 0$ .

*Case 1:  $\omega = 0$ .* Substituting Equations (2) and (4) into Equation (5), we can derive the characteristic equation of the PI-NMM control system as follows

$$\Delta(s) = 1 + \left[ K_p + \frac{K_i}{s} \right] \left\{ \frac{\frac{H_e \tau_e}{(\tau_e s + 1)^2}}{1 + K_s^2 \frac{H_e \tau_e}{(\tau_e s + 1)^2} \left[ C_3 C_4 \frac{H_i \tau_i}{(\tau_e s + 1)^2} - C_1 C_2 \frac{H_e \tau_e}{(\tau_e s + 1)^2} \right]} \right\} = 0 \tag{7}$$

Let  $s = j\omega$ . Thus, Equation (7) can be rewritten as

$$\Delta(j\omega) = 1 + \left[ K_p + \frac{K_i}{j\omega} \right] \left\{ \frac{\frac{H_e \tau_e}{(j\tau_e \omega + 1)^2}}{1 + K_s^2 \frac{H_e \tau_e}{(j\tau_e \omega + 1)^2} \left[ C_3 C_4 \frac{H_i \tau_i}{(j\tau_e \omega + 1)^2} - C_1 C_2 \frac{H_e \tau_e}{(j\tau_e \omega + 1)^2} \right]} \right\} = 0, \tag{8}$$

For  $\omega = 0$ , Equation (8) can be simplified as

$$1 + \left[ K_p + \frac{K_i}{j\omega} \right] \left\{ \frac{H_e \tau_e}{1 + K_s^2 H_e \tau_e (C_3 C_4 H_i \tau_i - C_1 C_2 H_e \tau_e)} \right\} = 0$$

We can derive

$$K_i = -j\omega \left[ \frac{1 + K_s^2 H_e \tau_e (C_3 C_4 H_i \tau_i - C_1 C_2 H_e \tau_e)}{H_e \tau_e} + K_p \right].$$

Thus, we can obtain the stability boundary for the case  $\omega = 0$ , i.e.,  $H_1$ , as follows:

$$K_i = 0 \tag{9}$$

This equation is a line in the  $(K_p, K_i)$  plane that is shown in Fig. 3 (the purple line).

Next, according to Equation (7), we can further derive the characteristic equation of the PI-NMM control system as follows:

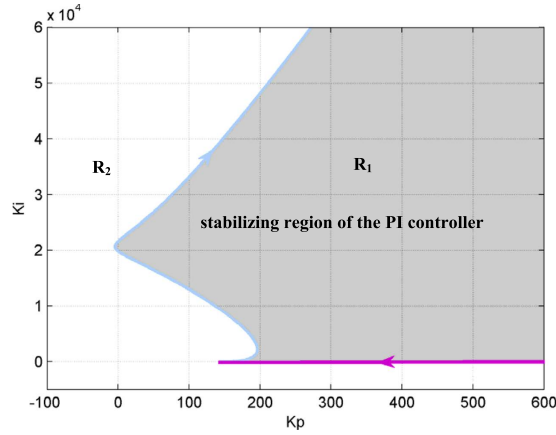


**Figure 3. The stabilizing region of the PI controller to suppress epileptic activity in the NMM ( $H_e = 4.5 \text{ mV}$ ).** The arrows represent the direction of the curve  $(K_p(\omega), K_i(\omega))$  in which  $\omega$  increases. The light blue curve is defined by Equation (13), and the purple line is defined by Equation (9). The parameter space to the right of the curve and above the line is the stabilizing region of the PI controller.

$$s(\tau_e s + 1)^4 (\tau_i s + 1)^2 + sK_s^2 H_e \tau_e [C_3 C_4 H_i \tau_i (\tau_e s + 1)^2 - C_1 C_2 H_e \tau_e (\tau_i s + 1)^2] + (sK_p + K_i) [H_e \tau_e (\tau_e s + 1)^2 (\tau_i s + 1)^2] = 0$$

Note that the coefficient of  $s^7$  in the characteristic polynomial, i.e.,  $\tau_e^4 \tau_i^2$ , is positive. According to the Routh stability criterion<sup>47</sup>, if the system is stable, then all of the coefficients of the characteristic equation should have the same sign. The constant term should also be positive, i.e.,  $K_i H_e \tau_e > 0$ . Thus, it follows that

$$K_i > 0, \tag{10}$$

Therefore, we can obtain the following lemma 1.

**Lemma 1** For the case  $\omega = 0$ , the region above the  $K_i$  axis in the  $(K_p, K_i)$  plane is the stabilizing region of the PI controller.

*Case 2:  $\omega = 0$ .* Supposing that  $\delta_{R\_NMM}(\omega)$  and  $\delta_{I\_NMM}(\omega)$  are the real and the imaginary components of  $G_{NMM}(j\omega)$ , respectively, then Equation (6) can be rewritten as

$$\begin{aligned} \Delta(j\omega) &= 1 + \left[ K_p + \frac{K_i}{j\omega} \right] [\delta_{R\_NMM}(\omega) + j\delta_{I\_NMM}(\omega)] \\ &= 1 + K_p \delta_{R\_NMM}(\omega) + \frac{K_i}{\omega} \delta_{I\_NMM}(\omega) \\ &\quad + j \left[ K_p \delta_{I\_NMM}(\omega) - \frac{K_i}{\omega} \delta_{R\_NMM}(\omega) \right] = 0 \end{aligned} \tag{11}$$

Equation (11) can be split into the following two parts

$$\begin{cases} \delta_R(\omega) = 1 + K_p \delta_{R\_NMM}(\omega) + \frac{K_i}{\omega} \delta_{I\_NMM}(\omega) = 0 \\ \delta_I(\omega) = K_p \delta_{I\_NMM}(\omega) - \frac{K_i}{\omega} \delta_{R\_NMM}(\omega) = 0 \end{cases}, \tag{12}$$

where  $\delta_R(\omega)$  and  $\delta_I(\omega)$  are the real and imaginary components of  $\Delta(j\omega)$ , respectively.

Note that both  $\delta_R(\omega)$  and  $\delta_I(\omega)$  are dependent on  $K_p$  and  $K_i$ . Thus, the stability of the characteristic Equation (12) can be investigated in the parameter space  $(K_p, K_i)$ .

According to Equation (12), we can further derive

$$\begin{cases} K_i = K_i(\omega) = \frac{\omega \delta_{I\_NMM}(\omega)}{[\delta_{R\_NMM}(\omega)]^2 + [\delta_{I\_NMM}(\omega)]^2} = \frac{\omega \delta_{I\_NMM}(\omega)}{|G_{NMM}(j\omega)|^2} \\ K_p = K_p(\omega) = - \frac{\delta_{R\_NMM}(\omega)}{[\delta_{R\_NMM}(\omega)]^2 + [\delta_{I\_NMM}(\omega)]^2} = - \frac{\delta_{R\_NMM}(\omega)}{|G_{NMM}(j\omega)|^2} \end{cases} \tag{13}$$

where  $|G_{NMM}(j\omega)| = \sqrt{\delta_{I\_NMM}^2(\omega) + \delta_{R\_NMM}^2(\omega)}$  is the complex modulus of  $G_{NMM}(j\omega)$ .



Equation (13) defines the stabilizing region  $H_2$  of the PI controller in the  $(K_p, K_i)$  plane for the case  $\omega > 0$ . According to Equation (13), we can draw the stability boundary curve  $(K_p(\omega), K_i(\omega))$  for  $\omega > 0$ , as shown in Fig. 3 (the light blue curve).

According to Equation (1), the stability boundary is composed of the stability boundary line defined by Equation (9) and the stability boundary curve defined by Equation (13). As illustrated in Fig. 3, the stability line and the stability boundary curve divide the  $(K_p, K_i)$  plane into two regions, which are denoted  $R_1$  and  $R_2$ , respectively. In the following section, we investigate which is the stabilizing region of the PI controller.

Next, we introduce the following proposition<sup>56</sup>. If one travelled along the curve defined by  $H_2$  in the direction of increasing  $\omega$ , then the right side is the stabilizing parameter region where  $\det J < 0$  and the left is where  $\det J > 0$ . Here,  $J$  is the Jacobian matrix defined as

$$J = \begin{bmatrix} \frac{\partial \delta_R(\omega)}{\partial K_p} & \frac{\partial \delta_R(\omega)}{\partial K_i} \\ \frac{\partial \delta_I(\omega)}{\partial K_p} & \frac{\partial \delta_I(\omega)}{\partial K_i} \end{bmatrix}, \tag{14}$$

From Equation (12), we obtain  $\frac{\partial \delta_R(\omega)}{\partial K_p} = \delta_{R\_NMM}(\omega)$ ,  $\frac{\partial \delta_R(\omega)}{\partial K_i} = \frac{\delta_{I\_NMM}(\omega)}{\omega}$ ,  $\frac{\partial \delta_I(\omega)}{\partial K_p} = \delta_{I\_NMM}(\omega)$  and  $\frac{\partial \delta_I(\omega)}{\partial K_i} = -\frac{\delta_{R\_NMM}(\omega)}{\omega}$ .

Substituting the above four equations into Equation (14), we can obtain  $\det J = -\frac{|G_{NMM}(j\omega)|^2}{\omega}$ . Because  $\omega > 0$  and  $|G_{NMM}(j\omega)|^2 > 0$ , it follows that

$$\det J < 0, \tag{15}$$

Therefore, we derive the following lemma 2.

**Lemma 2** For the case  $\omega > 0$ , following the curve  $(K_p(\omega), K_i(\omega))$  in the direction of increasing  $\omega$ , the parameter space to the right of the curve defined by Equation (13) is the stabilizing region of the PI controller.

**Main theoretical results.** Combining Lemma 1 with Lemma 2 yields the following theorem.

**Theorem 1** For the PI-NMM control system depicted in Fig. 2, the exact stabilizing parameter region of the PI controller is the parameter space above the line defined by Equation (9) and to the right of the curve defined by Equation (13) if it is followed in the direction of increasing  $\omega$ .

Thus, according to Theorem 1, the region denoted by  $R_1$  in Fig. 3 was identified as the stabilizing region of parameters  $(K_p, K_i)$ , and  $R_2$  was the destabilizing parameter region.

**Effect of excitatory and inhibitory NMM parameters on the stabilizing region of the PI controller.**

Epileptic activity is caused by the imbalance of excitation and inhibition in the NMM, which is caused by extremely large excitatory,  $H_e$ , or small inhibitory parameters,  $H_i$ , respectively. Therefore, we discussed the effect of the two parameters on the stabilizing region of the PI controller.

Figures 4 and 5 illustrate the stabilizing regions of the NMM PI controller for different abnormal values of  $H_e$  and  $H_i$ , respectively. Figures 4B and 5B show the stabilizing region of the PI controller for small values of the integral coefficient,  $K_i$ . The results demonstrate that the stabilizing region of the PI controller becomes smaller with increasing  $H_e$  (hyper-excitation) and decreasing  $H_i$  (low inhibition).

**Theoretical results of the steady-state performance analysis.** According to Fig. 2C, we can derive the closed-loop transfer function of the PI-NMM from the input,  $r(t)$ , to the error signal,  $e(t)$ , as

$$\phi_e(s) = \frac{E(s)}{R(s)} = \frac{1}{1 + G_{pi}(s)G_{NMM}(s)}, \tag{16}$$

where  $E(s)$  and  $R(s)$  are the Laplace transforms of  $e(t)$  and  $r(t)$ , respectively. According to Equation (16), one can obtain

$$E(s) = R(s)\phi_e(s) \tag{17}$$

In this study, the desired output of the PI-NMM was set to a constant value,  $r(t) = a$ , and its Laplace transform is derived as follows:

$$R(s) = a/s, \tag{18}$$

Substituting Equations (16) and (18) into Equation (17), we further obtain

$$E(s) = \frac{a}{s} \frac{1}{1 + G_{pi}(s)G_{NMM}(s)}, \tag{19}$$

According to feedback control principles<sup>47</sup>, the control error at steady state,  $e_{ss}$ , is as follows:

$$e_{ss} = \lim_{t \rightarrow \infty} e(t) = \lim_{s \rightarrow 0} sE(s) \tag{20}$$

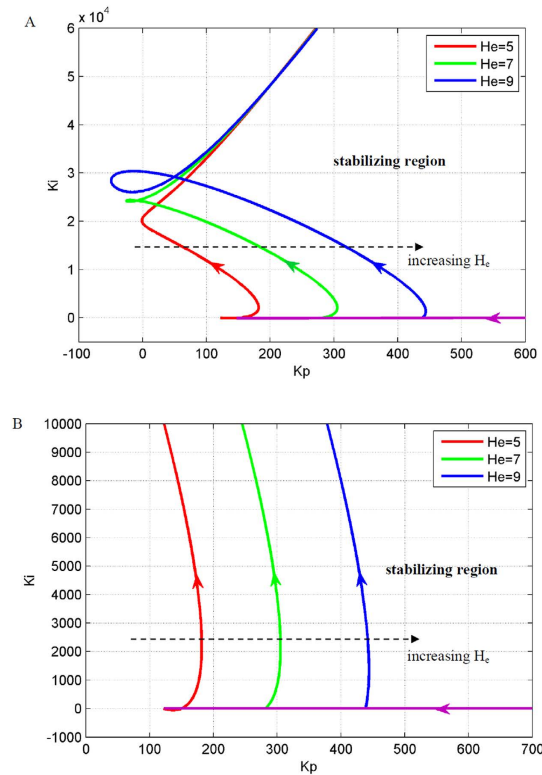


**Figure 4.** The effect of excitatory parameter,  $H_e$ , on the stabilizing region of the PI controller, (B) is an enlarged version of (A). The parameter space to the right of the red, green and blue curves are the stabilizing region of the PI controller for suppressing epileptic activity in the NMM with  $H_e = 5, 7$  and  $9$ , respectively.

Substituting Equations (2), (4) and (19) into Equation (20), we derive

$$e_{ss} = \lim_{s \rightarrow 0} s \cdot \frac{a}{s} \cdot \frac{1}{1 + \left[ K_p + \frac{K_i}{s} \right] \left\{ \frac{\frac{H_e \tau_e}{(\tau_e s + 1)^2}}{1 + K_s^2 \frac{H_e \tau_e}{(\tau_e s + 1)^2} \left[ C_3 C_4 \frac{H_i \tau_i}{(\tau_i s + 1)^2} - C_1 C_2 \frac{H_e \tau_e}{(\tau_e s + 1)^2} \right]} \right\}} = 0, \tag{21}$$

which shows that the output,  $y(t)$ , of the NMM is equal to the desired output,  $r(t)$ , at steady state.

In this study, we set  $r(t) = a = 0$ ; in this case, Equation (21) still holds. This result indicates that the PI controller can achieve an error-free control performance at steady-state and, thus, successfully suppresses epileptic activity in the NMM. It should be noted that the input of the NMM was noise signal; therefore, the PI-NMM control system could not be operated at steady-state<sup>57</sup> and a small control error existed, as shown in Figs. 6 and 7.

**Simulation results.** Simulations were conducted to illustrate the efficiency of the proposed PI control scheme to suppress epileptic activity in the NMM. We simulated the following two cases: hyper-excitation ( $H_e = 7.0$  mV) and low inhibition ( $H_i = 17.0$ ). According to Figs. 4 and 5, we determined the parameter values of the PI controller to be  $K_p = 310$  and  $K_i = 2$  for the hyper-excitation case and  $K_p = 90$  and  $K_i = 2$  for the low-inhibition case, respectively. The simulation results are illustrated in Figs. 6 and 7. The results showed that the output of the NMM without the PI controller was high-amplitude epileptic activity, which became low-amplitude activity under the control of the PI controller. Thus, the high-amplitude epileptic activities were successfully suppressed by the designed PI controller.

**Limitations.** To determine the stabilizing region of the PI controller, we used the graphical stability analysis method and conducted a linearized approximation of the NMM sigmoid function, which is extensively used in previous NMM studies<sup>27,46,58–60</sup>. It should be noted that the linearized approximation may provide a conservative estimate of the PI controller stabilizing region. In the future, a non-linear method, such as the bifurcation analysis method<sup>28,42,43,45</sup>, should be employed to determine a more specific stabilizing region for the proposed PI-based control scheme.

### Conclusions

In the present study, we used Jansen’s neural mass model as a test bed to develop a systematic design approach to determine the control parameters of a PI controller. It should be noted that the proposed design method of the



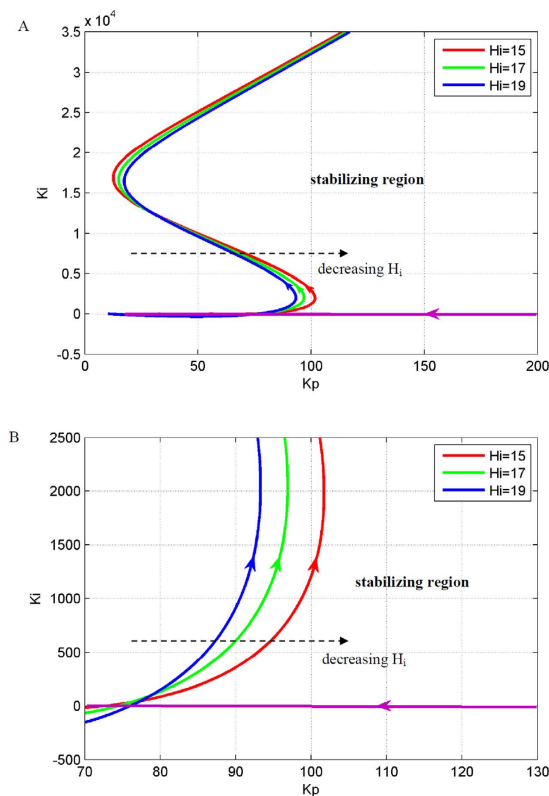


**Figure 5.** The effect of inhibitory parameter,  $H_i$ , on the stabilizing region of the PI controller, **(B)** is an enlarged version of **(A)**. The parameter space to the right of the red, green and blue curves are the stabilizing region of the PI controller for suppressing epileptic activity in the NMM with  $H_i = 15, 17$  and  $19$ , respectively.

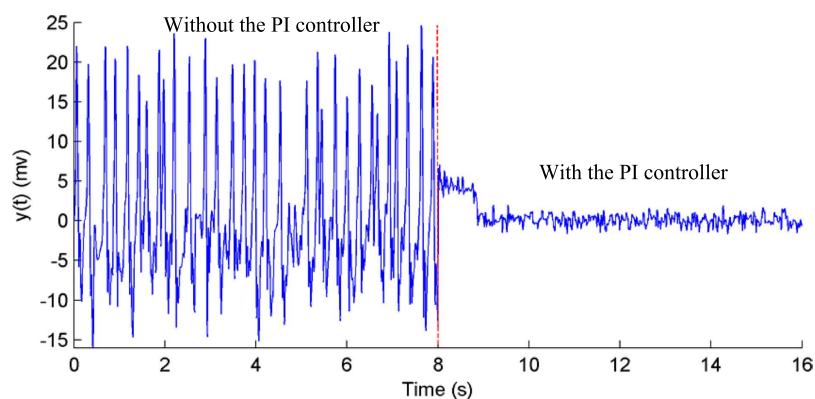


**Figure 6.** The output of the NMM without (before the eighth second) and with (after the eighth second) the PI controller during hyper-excitation ( $H_e = 7.0$ ).

PI controller was independent of a specific model. Thus, it can be extended to other neural models<sup>37,40,45,46,50–55</sup>, such as the epileptic activity model developed by Wendling *et al.*<sup>40</sup>, and other low-order closed-loop controllers<sup>24–31</sup>, such as the proportional controller and the proportional-derivative controller. Here, we took a parametric approach to seizure behaviour to demonstrate how to use the PI controller to suppress epileptic activity. However, there are other factors that cause epilepsy<sup>1</sup> in addition to the excitatory and inhibitory parameters, such as the stimulus<sup>43,45</sup>. The design method and process were not dependent on the factors that cause epilepsy; thus, the proposed design method can be extended to other cases involving epileptic activity that is characterized as high-amplitude oscillations<sup>1,4,28,40,41,45,49,52</sup>.

A graphical stability analysis method was utilized to determine the stability region of the PI controller in the parameter space. This provided a region of the PI control parameters that would suppress epileptic activity in the NMM. The proposed method ensured that the design of the controller was analytical, enabled theoretical analysis and revealed cause and effect relationships in a theoretical manner. This allowed us to explore the relationship

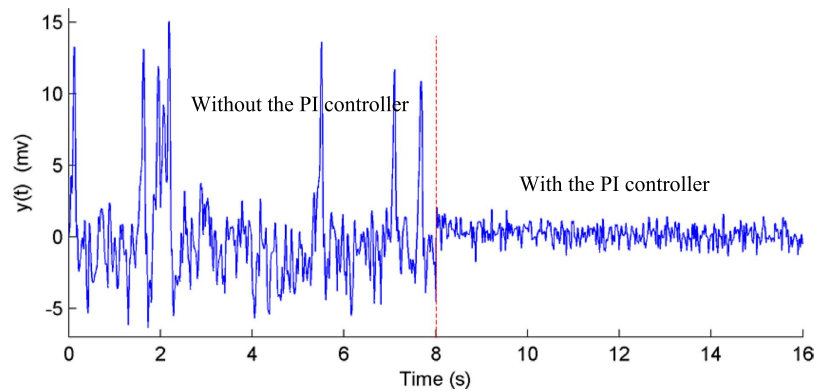


**Figure 7.** The output of the NMM without (before the eighth second) and with (after the eighth second) the PI controller during low inhibition ( $H_i = 17.0$ ).

between control parameters and model parameters that induced epileptic activity, which helped us understand the mechanism that suppresses neural diseases through closed-loop neurological electrical stimulation. In future work, we should attempt on-line seizure suppression by applying the proposed control scheme to standard animal models of epilepsy, with the long-term goal of applying it to human patients.

## References

- Lytton, W. W. Computer modelling of epilepsy. *Nat. Rev. Neurosci.* **9**, 626–637 (2008).
- Da Silva, F. L. *et al.* Epilepsies as dynamical diseases of brain systems: basic models of the transition between normal and epileptic activity. *Epilepsia* **44**, 72–83 (2003).
- Silva, F. H. *et al.* Dynamical diseases of brain systems: different routes to epileptic seizures. *IEEE. T. Bio-med. Eng.* **50**, 540–548 (2003).
- Jirsa, V. K., Stacey, W. C., Quilichini, P. P., Ivanov, A. I. & Bernard, C. On the nature of seizure dynamics. *Brain* **137**, 2210–2230 (2014).
- Jun-Song, W. & Yao, X. Spontaneous oscillation analysis of neural mass model using describing function approach. *Acta Phys. Sinch. Ed.* **63**, 68701, 1–8 (2014).
- Berényi, A., Belluscio, M., Mao, D. & Buzsáki, G. Closed-loop control of epilepsy by transcranial electrical stimulation. *Science* **337**, 735–737 (2012).
- Carron, R., Chaillet, A., Filipchuk, A., Pasillas-Lépine, W. & Hammond, C. Closing the loop of deep brain stimulation. *Front. Syst. Neurosci.* **7**, 00112, doi: 10.3389/fnsys.2013.00112 (2013).
- Paz, J. T. *et al.* Closed-loop optogenetic control of thalamus as a tool for interrupting seizures after cortical injury. *Nat. Neurosci.* **16**, 64–70 (2013).
- Rosin, B. *et al.* Closed-loop deep brain stimulation is superior in ameliorating parkinsonism. *Neuron* **72**, 370–384 (2011).
- Santaniello, S., Fiengo, G., Glielmo, L. & Grill, W. M. Closed-loop control of deep brain stimulation: a simulation study. *IEEE. T. Neur. Sys. Reh.* **19**, 15–24 (2011).
- Schiff, S. J. *Neural control engineering: the emerging intersection between control theory and neuroscience*. MIT Press (2012).
- Luo, M. & Xu, J. Suppression of collective synchronization in a system of neural groups with washout-filter-aided feedback. *Neural Networks* **24**, 538–543 (2011).
- Colic, S., Zalay, O. C. & Bardakjian, B. L. Responsive neuromodulators based on artificial neural networks used to control seizure-like events in a computational model of epilepsy. *Int. J. Neural. Syst.* **21**, 367–383 (2011).
- Nabi, A., Mirzadeh, M., Gibou, F. & Moehlis, J. Minimum energy desynchronizing control for coupled neurons. *J. Comput. Neurosci.* **34**, 259–271 (2013).
- Rhew, H.-G. *et al.* A Fully Self-Contained Logarithmic Closed-Loop Deep Brain Stimulation SoC With Wireless Telemetry and Wireless Power Management. *IEEE. J. Solid-st. Circ* **49**, 2213–2227 (2014).
- Almeida, L. *et al.* Chasing tics in the human brain: development of open, scheduled and closed loop responsive approaches to deep brain stimulation for tourette syndrome. *J. Clin. Neurol.* **11**, 122–131 (2015).
- Johnson, M. D. *et al.* Neuromodulation for brain disorders: challenges and opportunities. *IEEE. T. Bio-med. Eng.* **60**, 610–624 (2013).
- Grahn, P. J. *et al.* A neurochemical closed-loop controller for deep brain stimulation: toward individualized smart neuromodulation therapies. *Front. Neurosci.* **8**, 00169, doi: 10.3389/fnins.2014.00169 (2014).
- Åström, K. J. & Hägglund, T. The future of PID control. *Control Eng. Pract.* **9**, 1163–1175 (2001).
- Chakravarthy, N., Sabesan, S., Tsakalis, K. & Iasemidis, L. Controlling epileptic seizures in a neural mass model. *J. Comb. Optim.* **17**, 98–116 (2009).
- Ma, Z., Zhou, W., Geng, S., Yuan, Q. & Li, X. Synchronization regulation in a model of coupled neural masses. *Biol. Cybern.* **107**, 131–140 (2013).
- Liu, X., Liu, H., Tang, Y. & Gao, Q. Fuzzy PID control of epileptiform spikes in a neural mass model. *Nonlinear Dynam.* **71**, 13–23 (2013).
- Luo, M., Wu, Y. & Peng, J. Washout filter aided mean field feedback desynchronization in an ensemble of globally coupled neural oscillators. *Biol. Cybern.* **101**, 241–246 (2009).
- Gorzelic, P., Schiff, S. & Sinha, A. Model-based rational feedback controller design for closed-loop deep brain stimulation of Parkinson's disease. *J. Neural. Eng.* **10**, 026016 (2013).
- Colpan, M. E., Li, Y., Dwyer, J. & Mogul, D. J. Proportional feedback stimulation for seizure control in rats. *Epilepsia* **48**, 1594–1603 (2007).
- Lopour, B. A. & Szeri, A. J. A model of feedback control for the charge-balanced suppression of epileptic seizures. *J. Comput. Neurosci.* **28**, 375–387 (2010).
- Modolo, J. *et al.* Using a virtual cortical module implementing a neural field model to modulate brain rhythms in Parkinson's disease. *Front. Neurosci.* **4**, 00045, doi: 10.3389/fnins.2010.00045 (2010).

28. Kramer, M. A., Lopour, B. A., Kirsch, H. E. & Szeri, A. J. Bifurcation control of a seizing human cortex. *Phys. Rev. E* **73**, 041928 (2006).
29. Koppert, M., Kalitzin, S., Velis, D., Da Silva, F. L. & Viergever, M. A. Reactive control of epileptiform discharges in realistic computational neuronal models with bistability. *Int. J. Neural. Syst.* **23**, 1250032 (2013).
30. Rosenblum, M. & Pikovsky, A. Delayed feedback control of collective synchrony: an approach to suppression of pathological brain rhythms. *Phys. Rev. E* **70**, 041904 (2004).
31. Modolo, J., Legros, A., Thomas, A. W. & Beuter, A. Model-driven therapeutic treatment of neurological disorders: reshaping brain rhythms with neuromodulation. *Interface Focus*, **1**, 61–74 (2010).
32. Žiburkus, J., Cressman, J. R. & Schiff, S. J. Seizures as imbalanced up states: excitatory and inhibitory conductances during seizure-like events. *Int. J. Neurobiol.* **109**, 1296–1306 (2013).
33. Suffczynski, P., Wendling, F., Bellanger, J.-J. & Da Silva, F. H. L. Some insights into computational models of (patho) physiological brain activity. *P. IEEE*, **94**, 784–804 (2006).
34. Deco, G., Jirsa, V. K., Robinson, P. A., Breakspear, M. & Friston, K. The dynamic brain: from spiking neurons to neural masses and cortical fields. *PLoS Comput. Biol.* **4**, e1000092 (2008).
35. Gerstner, W., Sprekeler, H. & Deco, G. Theory and simulation in neuroscience. *Science* **338**, 60–65 (2012).
36. Nevado-Holgado, A. J., Marten, F., Richardson, M. P. & Terry, J. R. Characterising the dynamics of EEG waveforms as the path through parameter space of a neural mass model: application to epilepsy seizure evolution. *Neuroimage* **59**, 2374–2392 (2012).
37. Zandt, B.-J., Visser, S., van Putten, M. J. & ten Haken, B. A neural mass model based on single cell dynamics to model pathophysiology. *J. Comput. Neurosci.* **37**, 549–568 (2014).
38. Becker, R., Knock, S., Ritter, P. & Jirsa, V. Relating alpha power and phase to population firing and hemodynamic activity using a thalamo-cortical neural mass model. *PLoS Comput. Biol.* **11**, e1004352 (2015).
39. Youssofzadeh, V., Prasad, G. & Wong-Lin, K. On self-feedback connectivity in neural mass models applied to event-related potentials. *NeuroImage* **108**, 364–376 (2015).
40. Wendling, F., Bartolomei, F., Bellanger, J. & Chauvel, P. Epileptic fast activity can be explained by a model of impaired GABAergic dendritic inhibition. *Eur. J. Neurosci.* **15**, 1499–1508 (2002).
41. Touboul, J., Wendling, F., Chauvel, P. & Faugeras, O. Neural mass activity, bifurcations, and epilepsy. *Neural. Comput.* **23**, 3232–3286 (2011).
42. Xiao-Fei, X. & Jun-Song, W. Influence of synaptic plasticity on dynamics of neural mass model: a bifurcation study. *Acta Phys. Sin.* **63**, 140503, 1–10 (2014).
43. Spiegler, A., Kiebel, S. J., Atay, F. M. & Knösche, T. R. Bifurcation analysis of neural mass models: Impact of extrinsic inputs and dendritic time constants. *Neuroimage* **52**, 1041–1058 (2010).
44. Jansen, B. H. & Rit, V. G. Electroencephalogram and visual evoked potential generation in a mathematical model of coupled cortical columns. *Biol. Cybern.* **73**, 357–366 (1995).
45. Grimbert, F. & Faugeras, O. Bifurcation analysis of Jansen's neural mass model. *Neural. Comput.* **18**, 3052–3068 (2006).
46. Ursino, M., Cona, F. & Zavaglia, M. The generation of rhythms within a cortical region: analysis of a neural mass model. *NeuroImage* **52**, 1080–1094 (2010).
47. Franklin, G. F., Powell, J. D. & Emami-Naeini, A. Feedback control of dynamics systems. *Addison-Wesley, Reading, MA* (1994).
48. Hwang, C. & Hwang, J.-H. Stabilisation of first-order plus dead-time unstable processes using PID controllers. *Iee. P-contr. Theor. Ap* **151**, 89–94 (2004).
49. Goodfellow, M., Schindler, K. & Baier, G. Intermittent spike-wave dynamics in a heterogeneous, spatially extended neural mass model. *Neuroimage* **55**, 920–932 (2011).
50. Kalitzin, S., Koppert, M., Petkov, G. & Da Silva, F. L. Multiple oscillatory states in models of collective neuronal dynamics. *Int. J. Neural. Syst.* **24**, 1450020 (2014).
51. Koppert, M., Kalitzin, S., Velis, D., Lopes Da Silva, F. & Viergever, M. A. Dynamics of collective multi-stability in models of multi-unit neuronal systems. *Int. J. Neural. Syst.* **24**, 1430004 (2014).
52. Goodfellow, M., Schindler, K. & Baier, G. Self-organised transients in a neural mass model of epileptogenic tissue dynamics. *NeuroImage* **59**, 2644–2660 (2012).
53. Papadopoulou, M. *et al.* Tracking slow modulations in synaptic gain using dynamic causal modelling: validation in epilepsy. *Neuroimage* **107**, 117–126 (2015).
54. Koppert, M., Kalitzin, S., da Silva, F. L. & Viergever, M. Plasticity-modulated seizure dynamics for seizure termination in realistic neuronal models. *J. Neural. Eng.* **8**, 046027 (2011).
55. Suffczynski, P., Kalitzin, S. & Da Silva, F. L. Dynamics of non-convulsive epileptic phenomena modeled by a bistable neuronal network. *Neuroscience* **126**, 467–484 (2004).
56. Diekmann, O., van Gils, S., Lunel, S. V. & WALTHER, H., *Delay Equations: Functional, Complex, and Nonlinear Analysis* Springer-Verlag, New York (1995).
57. Rabinovich, M., Huerta, R. & Laurent, G. Transient dynamics for neural processing. *Science* **321**, 48–50 (2008).
58. David, O. & Friston, K. J. A neural mass model for meg/eeeg: coupling and neuronal dynamics. *NeuroImage* **20**, 1743–1755 (2003).
59. Babajani-Feremi, A. & Soltanian-Zadeh, H. Multi-area neural mass modeling of EEG and MEG signals. *Neuroimage* **52**, 793–811 (2010).
60. Modolo, J., Edwards, R., Campagnaud, J., Bhattacharya, B. & Beuter, A. Past, present and future of brain stimulation. *Math. Model. Nat. Phenom.* **5**, 185–207 (2010).

## Acknowledgements

This study was supported by the National Natural Science Foundation of China (Nos 61473208, 61025019, and 91132722), ONR MURI N000141010278 and NIH grant R01EY016281.

## Author Contributions

J.W. and X.L. conceived and designed the research. J.W. and E.N. performed the theoretical analysis. J.W. and J.H. performed the simulation analysis. J.W. wrote the main manuscript text. All authors reviewed the manuscript.

## Additional Information

**Competing financial interests:** The authors declare no competing financial interests.

**How to cite this article:** Wang, J. *et al.* Suppressing epileptic activity in a neural mass model using a closed-loop proportional-integral controller. *Sci. Rep.* **6**, 27344; doi: 10.1038/srep27344 (2016).



This work is licensed under a Creative Commons Attribution 4.0 International License. The images or other third party material in this article are included in the article's Creative Commons license, unless indicated otherwise in the credit line; if the material is not included under the Creative Commons license, users will need to obtain permission from the license holder to reproduce the material. To view a copy of this license, visit <http://creativecommons.org/licenses/by/4.0/>